Journal of Thermal Biology 82 (2019) 213–221

Contents lists available at ScienceDirect

Journal of Thermal Biology

journal homepage: www.elsevier.com/locate/jtherbio

Generalized solution and estimation method for cooling performance of downscaled cryoprobe

Junnosuke Okajima

Institute of Fluid Science, Tohoku University, 2-1-1, Katahira, Aoba-ku, Sendai, Miyagi, 980-8577, Japan

ARTICLE INFO

Keywords:
Cryosurgery
Cryoprobe
Dimensionless solution
Biot number
Dimensionless temperature

ABSTRACT

In cryosurgery, downscaling of cryoprobes is important to minimize surgical invasion. In this study, a set of analytical solutions to the freezing phenomenon around a cryoprobe in a dimensionless form is derived and the general trend is discussed to clarify the relationship between the freezing ability of a biological tissue and the cooling power of a cryoprobe. A one-dimensional axisymmetric model in the steady-state condition is considered. The relationship between the size of the frozen region, fluid temperature in the cryoprobe, and heat transfer coefficient on the wall of the cryoprobe in the dimensional form is derived under the condition mentioned above. The fluid temperature and heat transfer coefficient are eliminated from the solutions by introducing the steady-state cryoprobe surface temperature. This transformation indicates that the steady-state surface temperature directly affects the size of the frozen region and combination of fluid temperature and heat transfer coefficient occurs, which has the same cooling effect. The derived solutions are transformed into a dimensionless form using the characteristic length of bioheat transfer and normalizing the temperature distribution in an unfrozen tissue. The applicability of these analytical solutions is evaluated by comparing them with numerical simulation results from existing studies. The dimensionless solutions describe the general trend of the relationship between the frozen region and the cooling power of a cryoprobe, which is independent of the type of organ, fluid temperature, and heat transfer coefficient. Finally, the concept of freezing limit is established using the derived solutions. The freezing limit describes the minimum requirements to freeze a tissue, and it can be used as guideline to design future downscaled cryoprobes with a suitable cooling mechanism.

1. Introduction

Cryosurgery is a surgical treatment that uses intense freezing to destroy affected/unwanted tissues. Cryosurgery is advantageous in that it is less invasive, minimizes bleeding, and enables a short recovery period (Bischof et al., 1993). A cryoprobe is a cooling device for performing cryosurgery. A conventional cryoprobe is 3–8 mm in diameter and can be classified into two types according to the cooling method employed. One type of cryoprobe uses boiling flow of liquid nitrogen as the cooling mechanism (Popken et al., 2000). This type has an extremely high cooling power owing to the low boiling point of liquid nitrogen; however, vacuum insulation is required to maintain nitrogen in its liquid state, thus increasing the complexity of the system. The second type of cryoprobe uses the Joule–Thompson expansion of high-pressure gas (Coleman and Richardson, 2005; Forest et al., 2006). Several types of refrigerants (Fredrickson et al., 2006) are used for this type of cryoprobe; however, cryoprobes using the Joule–Thomson expansion have a low cooling efficiency. In this case, the surface temperature of a cryoprobe with a low heat transfer coefficient cannot reach the refrigerant temperature (Hewitt et al., 1997). Recently, cryosurgery has been used in the treatment of diseases such as prostate cancer, liver cancer, and lung cancer, as well as various skin conditions (Nikolai, 2007).

However, a conventional cryoprobe cannot be applied to lesions that are smaller than the diameter of the cryoprobe itself. Furthermore, some complications can arise due to injuries caused by the cryoprobe (Shimizu, 2004). Therefore, downscaling of the cryoprobe is required to extend the applications of cryosurgery to treating lesions. Miniature cryoprobes can be used to remove small, intricate lesions caused by conditions such as skin pigmentation and cancerous tumors. Some researchers have developed downscaled cryoprobes with diameters of 0.8 mm (Béita and Condé, 1972) and 0.9 mm (Zhang et al., 1986). However, these cryoprobes have insufficient cooling power for performing cryosurgery. The problem of a downscaled cryoprobe is the reduction of its cooling power due to the increase in its surface-area-to-volume (S/V) ratio.

To overcome this problem, the author has developed a 0.55-mm-diameter miniature surgical device referred to as an ultrafine cryoprobe

E-mail address: j.okajima@tohoku.ac.jp.

https://doi.org/10.1016/j.jtherbio.2019.04.010
Received 17 February 2019; Received in revised form 15 April 2019; Accepted 16 April 2019
Available online 21 April 2019

Nomenclature

Bi	Biot number
c	specific heat J/(kg·K)
h	heat transfer coefficient W/(m^2·K)
K_n	nth-order modified Bessel function of the second kind
k	thermal conductivity W/(m·K)
$k^{\dagger}$	thermal conductivity ratio
L	latent heat J/kg
Q	dimensionless heat flux
q	heat flux W/m^2
q_{met}	metabolic heat generation rate W/m^3
R	dimensionless coordinate of the radial direction
r	coordinate of the radial direction m
T	temperature K, ˚C
T_a	temperature of arterial blood K, ˚C
T_B	steady-state temperature of biological tissue K, ˚C
T_m	solidification temperature K, ˚C

Greek

δ_B	characteristic length of bioheat transfer m
θ	dimensionless temperature
ρ	density kg/m^3
ω_b	blood perfusion rate 1/s

Subscript

b	blood
F, f	frozen region
fluid	fluid in cryoprobe
p	probe
SS	steady-state probe-surface
UF	unfrozen region

(Okajima et al., 2014a). The targets of this device include small skin pigmentation with the size of few millimeters, early breast cancer with the size of less than 1 cm and performing cryosurgery in the blood vessel with a catheter. The miniature probe uses liquidized freon under high pressure and room temperature as the refrigerant and boiling heat transfer as the heat transfer mechanism. The ultrafine cryoprobe is advantageous in that it has no vacuum insulation and it has a higher cooling ability than probes using Joule–Thompson gas expansion. The flow pattern and heat transfer performance of the ultrafine cryoprobe were evaluated (Okajima et al., 2014b) and the transient freezing phenomenon was reproduced via numerical simulation (Okajima et al., 2014c). In addition, the thermodynamic properties of the new cryoprobe were calculated via numerical simulations and the effect of the probe's structure on the area of the frozen region was evaluated (Okajima et al., 2018). However, the limitation of downscaling the freezing ability of the probe has not been studied. Understanding the limitation is important to formulate guidelines for designing the cryoprobe. In particular, the relationship between the cooling power and the size of the cryoprobe should be investigated as the ratio of the surface area to the volume of the ultrafine cryoprobe is large.

Several researchers have analyzed the field of cryosurgery to predict or estimate the frozen region in a biological tissue. Numerical simulations are primarily used to predict the frozen area. For example, Zhang et al. (2005) conducted numerical simulations of prostate cancer cryosurgery; they used a complex three-dimensional geometry model to simulate the shape of the prostate gland. Nabaei and Mehardad (Nabaei and Karimi, 2018) conducted numerical simulation to evaluate the effect of blood vessels on the freezing process in a biological tissue. Furthermore, Chua et al. (2007) conducted numerical simulation of models for cryosurgery, including a cell destruction model. Hafid and Lacroix (2017) developed an inverse prediction method and estimated the thermophysical properties of a biological tissue. Hossain et al. (2018) and this author (Okajima et al., 2014c; Takeda et al., 2009) also conducted numerical simulation of the phenomena in cryosurgery including the heat transfer effects inside a cryoprobe. On the other hand, in separate studies, Cooper et al. (Cooper and Trezek, 1971) and Jiji et al. (Jiji and Ganatos, 2009) derived analytical solutions from the governing equation of the phase change phenomenon in a biological tissue. Deriving the analytical solutions can lead to better understanding of the relationships among the various parameters involved. However, these works focused on predicting the frozen region for a specific organ using a specific cryoprobe. Therefore, the relationship between the cooling power and the size of a cryoprobe, as well as the general characteristics of the probe, have not been clarified.

The objective of the present study is to clarify the relationship between the cooling performance and the size of the ultrafine cryoprobe by deriving the relevant analytical solutions. The cooling power of the cryoprobe was modeled using the boundary condition expressing convective heat transfer through the heat transfer coefficient and the temperature of the refrigerant. In addition, dimensionless parameters were introduced to the analytical solutions to clarify the general characteristics of that relationship. The general expressions and guideline to design the ultrafine cryoprobe are also discussed in this manuscript.

2. Working principle of ultrafine cryoprobe

Fig. 1 shows the schematic of the ultrafine cryoprobe and phase-change process of the refrigerant. The ultrafine cryoprobe has an outer diameter of 0.55 mm and a double-tube structure; an inner tube works as the pressure reducer or capillary and an outer tube works as the cooling section. At the inlet of the inner tube, the liquid refrigerant is supplied at high pressure and room temperature. The inner tube has a large flow resistance to strongly depressurize the refrigerant. Depressurization makes the refrigerant change to two-phase flow. Therefore, the outer tube, namely the cooling section, is cooled.

As a thermal problem, a downscaled cryoprobe, such as our ultrafine cryoprobe, is characterized by the probe radius and the cooling mechanism, which is determined by the fluid temperature and heat transfer ability of the fluid flow.

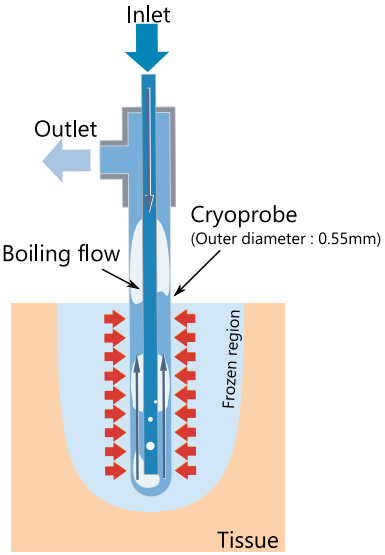

Fig. 1. Schematic of ultrafine cryoprobe and phase-change process of refrigerant.

3. Mathematical models

3.1. Equations and assumptions

Fig. 2 shows the schematic diagram of a one-dimensional axisymmetric analysis model. This model describes the frozen region that appears around a cryoprobe in a biological tissue. By assuming that the temperature distribution reaches a steady state, this system can be considered as a composite cylinder comprising frozen and unfrozen regions. A steady state model cannot operate on the transient process; however, it can help clarify the relationship between the maximum frozen size, heat transfer performance of fluid flow, and fluid temperature. The assumptions made for this study are as follows:

1. The transition region from the unfrozen to the frozen phase was not considered.
2. Heat conduction on the wall of the cryoprobe was neglected because of the difference between the thermal conductivities of metal and biological tissue.
3. Steady-state heat conduction was considered.
4. The solidification temperature of the biological tissue was fixed as −10 °C.
5. Bioheat generation in the frozen region was not considered.
6. The temperature dependence of thermophysical properties in each phase was not considered.

The bioheat transfer equation proposed by Pennes (1948) is used in this study as the governing equation for the unfrozen region at steady state, which is expressed as

$$\frac{k_{UF}}{r}\frac{d}{dr}\left[r\frac{dT_{UF}(r)}{dr}\right] + \rho_b c_b \omega_b [T_B - T_{UF}(r)] = 0 \quad : \quad r_f \le r \le \infty, \tag{1}$$

where T_B is the steady-state temperature of the biological tissue (Okajima et al., 2009), and is defined as

$$T_B = T_a + \frac{q_{met}}{\rho_b c_b \omega_b}, \tag{2}$$

where T_a denotes the temperature of arterial blood. The steady-state heat conduction equation is used as the governing equation for the frozen region, and is expressed as

$$\frac{k_F}{r}\frac{d}{dr}\left[r\frac{dT_F(r)}{dr}\right] = 0 \quad : \quad r_p \le r \le r_f, \tag{3}$$

where r_p denotes the radius of the cryoprobe. In general, the condition at the frozen–unfrozen region interface is expressed as

$$k_F \left.\frac{\partial T_F}{\partial r}\right|_{r=r_f} - k_{UF} \left.\frac{\partial T_{UF}}{\partial r}\right|_{r=r_f+dr_f} = \rho L \frac{dr_f}{dt}. \tag{4}$$

According to assumption 3, the heat flux interface condition between the frozen and unfrozen regions is expressed as

$$k_F \left.\frac{dT_F}{dr}\right|_{r=r_f} = k_{UF} \left.\frac{dT_{UF}}{dr}\right|_{r=r_f}. \tag{5}$$

In addition, the interface temperature is also satisfied by the following condition.

$$T_F(r_f) = T_{UF}(r_f) = T_m, \tag{6}$$

where T_m denotes the melting point. According to assumptions 1 and 4, the transition region between the frozen and unfrozen regions is not considered in this study. Furthermore, the boundary conditions on the cryoprobe's surface and at infinity are expressed as

$$-k_F \left.\frac{dT_F}{dr}\right|_{r=r_p} = h[T_{fluid} - T_F(r_p)], \tag{7}$$

$$T_{UF}(\infty) = T_B, \tag{8}$$

where h and T_{fluid} are the heat transfer coefficient and refrigerant temperature, respectively. The value of h indicates the flow state such as single or two-phase and laminar or turbulent. In addition, according to assumption 2, the convective heat flux by refrigerant flow inside the cryoprobe directly affects the surface of the frozen region; therefore, the heat flux on the surface of the frozen region is equal to the convective heat flux.

3.2. Dimensional solutions

The sets of analytical solutions were derived from the above equations. They consist of the temperature distribution in the frozen region, the temperature distribution in the unfrozen region, and the relational expression between the parameters, which are expressed as,

$$T_F(r) = T_m + (T_{fluid} - T_m)\frac{\ln(r/r_f)}{\ln(r_p/r_f) - \frac{k_F}{hr_p}}, \tag{9}$$

$$T_{UF}(r) = T_B + (T_m - T_B)\frac{K_0(r/\delta_B)}{K_0(r_f/\delta_B)}, \tag{10}$$

$$\frac{k_{UF}}{hr_p} = \frac{T_{fluid} - T_m}{T_m - T_B}\frac{\delta_B}{r_f}\frac{K_0(r_f/\delta_B)}{K_1(r_f/\delta_B)} + \frac{k_{UF}}{k_F}\ln\frac{r_p}{r_f}, \tag{11}$$

where K_n is the nth-order modified Bessel function of the second kind. Furthermore, δ_B is the characteristic length of bioheat transfer (Okajima et al., 2009), which is expressed as

$$\delta_B = \sqrt{\frac{k_{UF}}{\rho_b c_b \omega_b}}. \tag{12}$$

The derivation of Eq. (11) can be found in Ref. (Okajima et al., 2014a). The characteristic length of bioheat transfer, δ_B corresponds to the length for which thermal penetration occurs inside the biological tissue. Here, the concept used in Ref (Okajima et al., 2014a). to describe surface temperature is applied. Using Eq. (9), the steady-state probe-surface temperature can be described as

$$T_{SS} = T_m + (T_{fluid} - T_m)\frac{\ln(r_p/r_f)}{\ln(r_p/r_f) - \frac{k_F}{hr_p}}. \tag{13}$$

The steady-state probe-surface temperature, T_{SS} is an important parameter for this study. Using the T_{ss} expression in Eq. (13), Eqs. (9) and (11) are transformed into simpler forms, which are expressed as

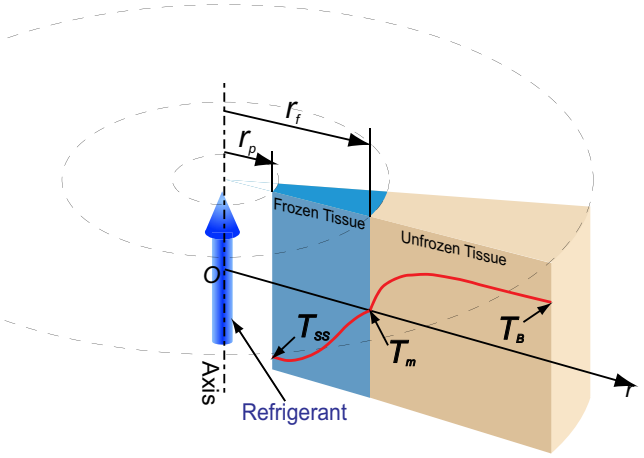

Fig. 2. Schematic diagram of one-dimensional axisymmetric bioheat transfer model with phase change.

$$T_F(r) = T_m + (T_{SS} - T_m)\frac{\ln(r/r_f)}{\ln(r_p/r_f)} \tag{14}$$

$$\frac{T_{SS} - T_m}{T_B - T_m}\frac{K_0(r_f/\delta_B)}{K_1(r_f/\delta_B)} + \frac{k_{UF}}{k_F}\frac{r_f}{\delta_B}\ln\frac{r_f}{r_p} = 0. \tag{15}$$

The heat transfer coefficient and refrigerant temperature in Eq. (15) are eliminated by introducing the steady-state probe-surface temperature, T_{SS}. Equation (15) shows the steady-state probe surface temperature and determines only the radius of the frozen region. This means that the heat transfer coefficient and refrigerant temperature indirectly affect the size of the frozen region through the steady-state probe-surface temperature. The steady-state surface temperature directly affects the size of the frozen region. Moreover, combination of the fluid temperature and the heat transfer coefficient occurs, which has the same cooling effect. In addition, the heat flux on the probe surface is also an important factor for evaluating the cooling performance. The heat flux on the probe surface at steady state, q_{SS} is defined as

$$q_{SS} = -k_F\frac{\partial T_F}{\partial r}\bigg|_{r=r_p} = -\frac{k_F(T_{SS} - T_m)}{r_p\ln(r_p/r_f)}. \tag{16}$$

In practice, Eq. (15) can predict the maximum size of the frozen region from the probe surface temperature, whereas Eq. (13) suggests selecting a combination of the heat transfer coefficient and the refrigerant temperature to determine the probe surface temperature. Together, these equations can be used as a design guide to develop a cryoprobe.

3.3. Dimensionless parameters and solutions

The equations in this section introduce dimensionless parameters into the analytical solutions derived in the previous section, to understand the general characteristics of the cooling power of a cryoprobe for performing cryosurgery. The author proposed a new dimensionless form of temperature independent of the factors/variables associated with various biological tissues analyzed in a previous study (Okajima et al., 2009). The analytical solutions contain three types of specific temperatures: the steady-state temperature of biological tissue, T_B; the solidification temperature, T_m; and the steady-state probe-surface temperature, T_{SS}. In this study, T_{SS} was selected as the variable parameter. Here, the dimensionless temperature, θ is defined as

$$\theta = \frac{T - T_m}{T_B - T_m}. \tag{17}$$

In Eq. (17), the dimensionless temperature becomes zero at the frozen boundary and unity at an infinite distance. Furthermore, the dimensionless coordinate, R and Biot number, Bi are expressed as

$$R = \frac{r}{\delta_B}, \tag{18}$$

$$Bi = \frac{h\delta_B}{k_F}. \tag{19}$$

The physical meaning of the dimensionless coordinate can be interpreted as the ratio of length to the characteristic length of the bioheat transfer, δ_B. This concept is valid in both the frozen and unfrozen regions. In addition, in physical terms, the Biot number describes the ratio of the convective heat transfer affecting the solid phase to the heat conduction in the solid phase. By introducing the Biot number, the essential process, which is independent of the type of tissue and the flow condition in the cryoprobe, can be discussed. Using the dimensionless parameters, the dimensionless steady-state probe-surface temperature, θ_{SS} transforms into the following equation:

$$\theta_{SS} = \theta_{fluid}\frac{\ln(R_p/R_f)}{\ln(R_p/R_f) - \frac{1}{Bi\cdot R_p}}. \tag{20}$$

Equation (20) shows that the dimensionless steady-state probe-surface temperature is determined by four dimensionless parameters, namely probe radius, frozen radius, refrigerant temperature, and Biot number. Moreover, Eqs. (9)–(11) and (16), respectively transform into the following equations:

$$\theta_F(R) = \theta_{SS}\frac{\ln(R/R_f)}{\ln(R_p/R_f)}, \tag{21}$$

$$\theta_{UF}(R) = 1 - \frac{K_0(R)}{K_0(R_f)}, \tag{22}$$

$$k^{\dagger}\theta_{SS}\frac{K_0(R_f)}{K_1(R_f)} + R_f\ln\frac{R_f}{R_p} = 0, \tag{23}$$

$$Q_{SS} = -k^{\dagger}\frac{\partial\theta_F}{\partial R}\bigg|_{R=R_p} = -\frac{k^{\dagger}\theta_{SS}}{R_p\ln(R_p/R_f)}, \tag{24}$$

where $k^{\dagger}$ represents the ratio of the thermal conductivity of the frozen tissue to that of the unfrozen tissue, which is expressed as

$$k^{\dagger} = \frac{k_F}{k_{UF}}. \tag{25}$$

The thermophysical properties of a biological tissue, except for the ratio of the thermal conductivity of the frozen tissue to that of the unfrozen tissue, are eliminated from the dimensionless solutions derived in this section. Therefore, these solutions represent the general cooling performance characteristics of a cryoprobe. The dimensionless solutions describe the general trend of the relationship between the frozen region and the cooling power of a cryoprobe, which is independent of the type of organ, fluid temperature, and heat transfer coefficient. Fig. 3 illustrates the steady-state temperature distribution in a biological tissue. The abscissa represents a dimensionless distance, which is defined as $R - R_p$. The inflection points indicate the positions of the frozen boundaries. As shown in Fig. 3, all the temperature distributions in the unfrozen region change in the range of 0–1, whereas the temperature distributions in the frozen region depend on the steady-state probe surface temperature. Therefore, the definition of the dimensionless temperature can accurately describe the general cooling performance characteristics of a cryoprobe.

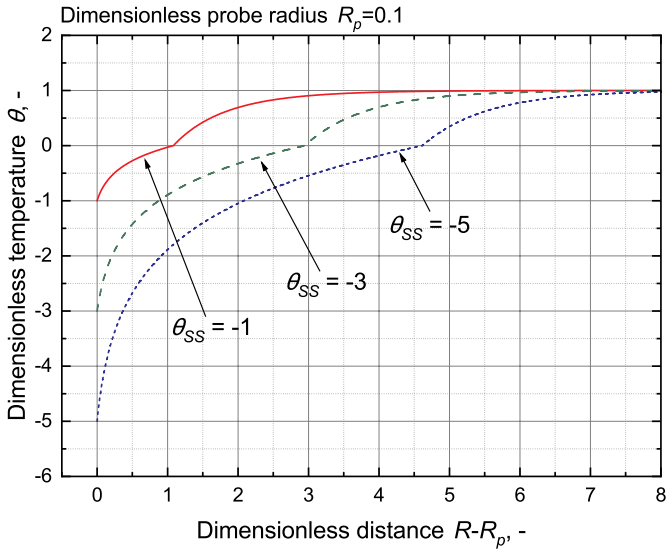

Fig. 3. Dimensionless steady-state temperature distribution in a biological tissue.

Table 1
Comparison with numerical simulation results obtained by Zhao et al. (2007)

Dimensional				Dimensionless			Relative difference [%]
$\rho_b c_b \omega_b$ [kW/(m^3·K)]	r_p [mm]	Solution [mm]	Literature (Zhao et al., 2007) [mm]	R_p	Solution	Literature (Zhao et al., 2007)	
10	1.50	24.33	17.00	0.21	3.44	2.40	43
20	1.50	19.27	15.90	0.30	3.85	3.18	21
40	1.50	15.05	13.80	0.42	4.26	3.90	9

4. Comparison with two-dimensional numerical simulation

The proposed solutions are validated by comparing them with the two-dimensional numerical simulation results from earlier studies. The validity of Eqs. (11) and (23) was confirmed using the numerical results obtained by Zhao et al. (2007) and Rabin et al. (Rabin and Shitzer, 1998). Zhao et al. calculated the time variation of the frozen region in a soft biological tissue with a 3-mm-diameter cryoprobe at −150 °C. They also investigated the effect of blood perfusion rate on the size of the frozen region. The sizes of the frozen region at 1000 s were compared with those obtained via the analytical solutions. Rabin et al. calculated the size of the frozen region by varying the probe radii. The cryoprobe temperature in that study was −196 °C. The calculated frozen region at 10 min was compared with those obtained via the analytical solution. The results of the comparison are listed in Tables 1 and 2.

As shown in Tables 1 and 2, the analytical solutions overestimated the size of the frozen region. The relative difference was defined as the ratio of the absolute difference to the value reported in the literature. As presented in Tables 1 and 2, the relative differences became smaller at larger values of the blood perfusion term $\rho_b c_b \omega_b$ and smaller probe radii. That is, the value from the analytical solution approaches that of the numerical simulation when the effect of bioheat is relatively large. The case of smaller probe radius also corresponds to relatively large bioheat effect.

One of the main reasons is the difference in the spatial dimension. The analytical solution assumed one-dimensional axisymmetry; heat was not allowed to flow in the axial (or depth) direction. Another major reason is the difference between steady-state and transient condition. The frozen region rapidly expanded in the early stage of cooling and the expansion rate became very small with time. Although the time variation of the frozen region is very small, steady-state was not achieved. Hence, the steady-state solution overestimated the value from the numerical simulation. In a real situation, the assumptions in this study should also account for the difference with respect to the analytical solution. In particular, the temperature dependence of thermal conductivity in the frozen region may affect the temperature distribution due to large temperature gradient around the cryoprobe. In addition, in the dimensionless case, the difference between the analytical solution and the numerical simulation is 1.2 ± 0.45. That is, the differences are 1.2 times the characteristic length of bioheat transfer; hence, the actual difference in each tissue is calculated using the value of the characteristic length of bioheat transfer as the average. The differences between the analytical solutions and the numerical results in this study are not sufficiently small to reproduce the phenomenon completely; however, this difference is considered to be acceptable to estimate the relationship between the cooling power of the cryoprobe and the size of the frozen region.

5. Results and discussion

5.1. Results of dimensionless solutions

Fig. 4(a) shows the relationship between the dimensionless frozen distance and probe radius, which is obtained from Eq. (23). In addition, Fig. 4(b) shows the relationship between the dimensionless heat flux and probe radius, which is obtained from Eq. (24). Here, the dimensionless temperatures −5, −4, −3, and −2, for example, represent the dimensional temperatures −225 °C, −178 °C, −131 °C, and −104 °C, respectively for the case where $T_m = -10$ °C and $T_B = 37$ °C. Furthermore, the dimensionless probe radius is defined as the ratio of the probe radius to the characteristic length of bioheat transfer, which is given in Eq. (12). This means that the dimensionless probe radius varies with the type of biological tissue.

As shown in Fig. 4(a), the dimensionless frozen distance decreases with the decrease in the dimensionless probe radius, regardless of the value of the dimensionless surface temperature. Therefore, to generate a frozen region of the same size, a smaller cryoprobe requires a lower surface temperature. Moreover, as shown in Fig. 4(b), the dimensionless heat flux drastically increases with the decrease in the dimensionless probe radius. Here, the ordinate in Fig. 4(b) is expressed on a logarithmic scale. Hence, a smaller cryoprobe is required to achieve a much larger heat transfer coefficient that can generate low temperatures.

Fig. 5 illustrates the relationship between the dimensionless refrigerant temperature and the Biot number, *Bi* for a dimensionless probe radius of 0.1. Fig. 5 can also be obtained using Eq. (20). As shown in Fig. 5, the surface temperature nearly reaches equilibrium with the refrigerant temperature when *Bi* is greater than 10^2. However, when *Bi* is less than 10^2, the surface temperature is greater than the refrigerant temperature.

Fig. 6 illustrates the relationship between the dimensionless refrigerant temperature and *Bi*, which produces a dimensionless probe

Table 2
Comparison with numerical simulation results obtained by Rabin et al. (Rabin and Shitzer, 1998).

Dimensional				Dimensionless			Relative difference [%]
$\rho_b c_b \omega_b$ [kW/(m^3·K)]	r_p [mm]	Solution [mm]	Literature (Rabin and Shitzer, 1998) [mm]	R_p	Solution	Literature (Rabin and Shitzer, 1998)	
40	1.00	17.27	13.50	0.28	4.88	3.82	28
	1.50	18.98	14.40	0.42	5.37	4.07	32
	2.50	21.45	15.70	0.71	6.07	4.44	37
	3.50	23.28	16.50	0.99	6.59	4.67	41
48.5	1.00	16.79	13.90	0.29	4.94	4.09	21
	1.50	18.47	14.90	0.44	5.43	4.35	24
	2.50	20.87	16.00	0.74	6.14	4.71	30
	3.50	22.65	17.30	1.03	6.67	5.09	31

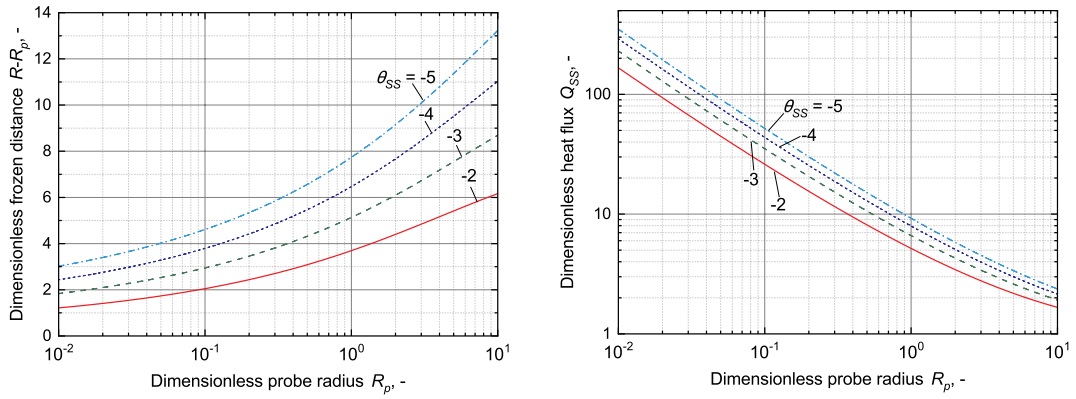

(a) Dimensionless frozen distance (b) Dimensionless heat flux

Fig. 4. Relationship between dimensionless probe radius and (a) dimensionless frozen distance and (b) dimensionless heat flux.

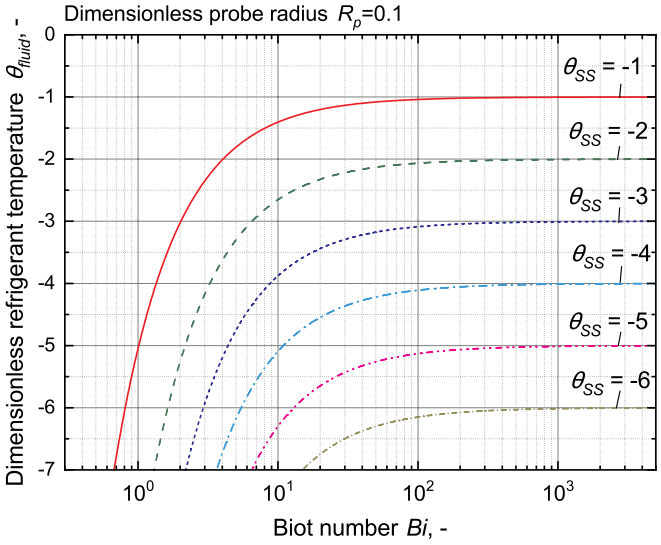

Fig. 5. Relationship between dimensionless refrigerant temperature and Biot number. (for dimensionless probe radius of 0.1).

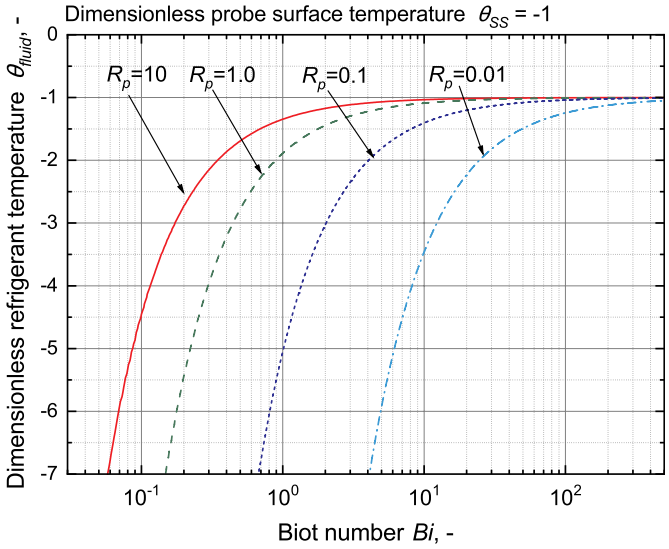

Fig. 6. Relationship between dimensionless refrigerant temperature and Biot number. (for dimensionless probe surface temperature of −1).

surface temperature of −1. Fig. 6 can also be obtained using Eq. (20). As shown in Fig. 4, the curves shift to the right as the dimensionless probe radius decreases. Specifically, a higher value of *Bi* is required for a smaller cryoprobe to generate the same cryoprobe surface temperature with the same refrigerant.

5.2. Minimum condition required to generate frozen region

When the cooling performance of the cryoprobe is insufficient, the frozen region cannot be generated. This temperature distribution can be derived by solving Eqs. (1), (7) and (8) with $r_f = 0$. The solution can be obtained as,

$$T_{UF}(r) = T_B + \frac{T_{fluid} - T_B}{1 + \frac{k_{UF}}{h\delta_B}\frac{K_1(r_p/\delta_B)}{K_0(r/\delta_B)}} \tag{26}$$

The general characteristics of this solution were discussed in our previous work (Okajima et al., 2009). In this paper, the required minimum cooling condition to generate a frozen region by cryoprobe is discussed.

Using these solutions, the general characteristics of the cooling ability of the new cryoprobe are discussed in the next section by transforming the dimensional temperature to its dimensionless form. Here, Eq. (26) is transformed to the dimensionless form as follows:

$$\theta_{UF}(R) = 1 + \frac{\theta_{fluid} - 1}{1 + \frac{1}{k^{\dagger}Bi}\frac{K_1(R_p)}{K_0(R)}} \tag{27}$$

The minimum required condition to freeze a biological tissue is that the cryoprobe surface temperature must be equal to the solidification temperature of the tissue. In its dimensionless form, $\theta = 0$ represents the solidification temperature. According to this discussion, the minimum required relationship between the refrigerant temperature, the Biot number, and the probe radius can be derived from Eq. (27), as follows:

$$\theta_{fluid} = -\frac{K_1(R_p)}{K_0(R_p)}\frac{1}{k^{\dagger}Bi} \tag{28}$$

Fig. 7 shows the relationship defined by Eq. (28) for dimensionless probe radius of 0.01. The line is defined by Eq. (28) and represents the freezing limit. The area above the line represents the conditions under which the frozen region cannot be generated, which means that these conditions are not suitable for the cryoprobe. In contrast, the area below the line represents the conditions under which the frozen region is generated, and the cryoprobe must satisfy these conditions.

Fig. 8 shows the relationship defined by Eq. (28) for an arbitrary probe radius. It is clear that miniature cryoprobes require higher *Bi* or lower refrigerant temperature to generate the frozen region. From Eq. (28), the difference in the probe radius is only determined by the

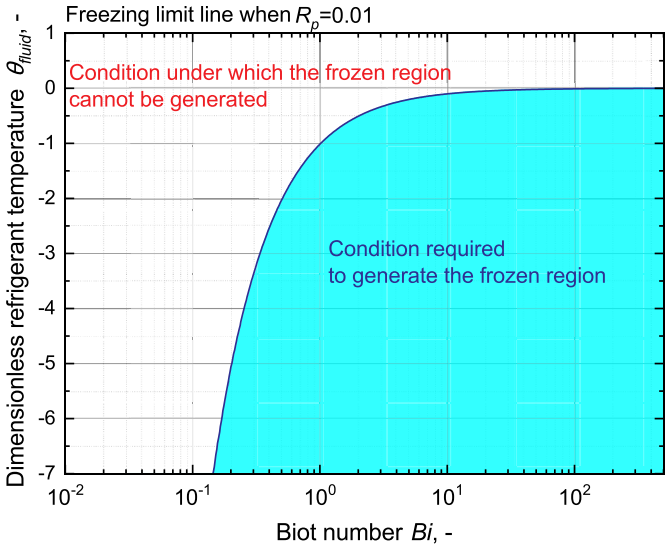

Fig. 7. Freezing limit for dimensionless probe radius = 0.01.

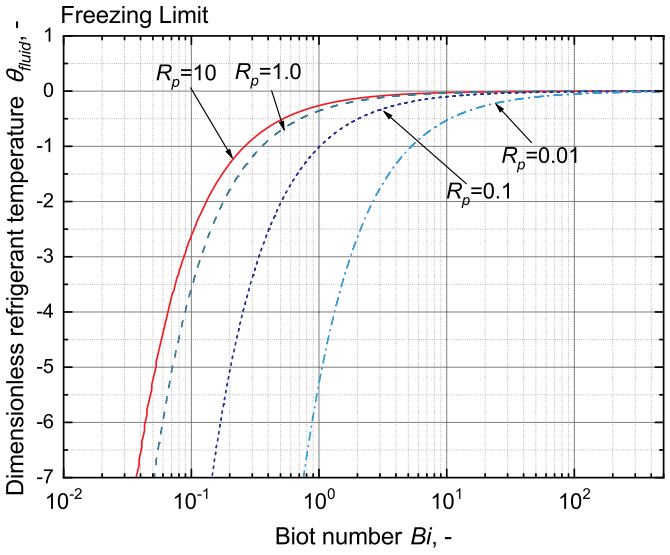

Fig. 8. Dimensionless freezing limit for various probe radii.

$K_1(R_p)/K_0(R_p)$ term. Therefore, when a given fluid temperature is considered, the values of the threshold Biot number are 2.84 and 14.8 times larger than those under R_p = 1.0 for probe radii of 0.1 and 0.01, respectively.

5.3. Examples of Dimensional Values

The results shown in the previous section can be transformed into dimensional results. The thermophysical properties of a typical soft tissue listed in Table 3 are used.

Fig. 9(a) illustrates the relationship between the frozen distance at steady state and the probe radius, whereas Fig. 9 (b) illustrates the relationship between the heat flux and the probe radius. As shown in Fig. 9(a), a lower probe surface temperature can generate a larger frozen region. However, even when the probe temperature is low, the frozen region becomes small as the probe radius decreases. For example, when the probe radius decreases from 10 mm to 0.1 mm, the radius of the frozen region decreases to less than half its original radius at all cryoprobe surface temperatures. Furthermore, when the size of the cryoprobe decreases, the heat flux increases as shown in Fig. 9 (b). For example, when the probe radius is 0.5 mm and the surface temperature is −50 °C, the steady-state heat flux reaches 70 kW/m^2. In the transient state, the heat flux, which the cryoprobe must remove, should be larger than that in the steady state. Therefore, a small cryoprobe is exposed to severe thermal restriction.

Fig. 10 shows the relationship between the refrigerant temperature and the heat transfer coefficient required to make the probe surface temperature reach −50 °C. As the probe radius decreases in size, the curves shift to the right. As such, a larger heat transfer coefficient is required to make the surface temperature of the smaller cryoprobe equal to that of the large cryoprobe. For example, when a refrigerant with boiling point of −100 °C is used and the probe radius is 1.5 mm, a heat transfer coefficient of 450 W/(m^2·K) is required to make the probe surface temperature reach −50 °C. Hence, single-phase gas flow is sufficient as a heat transfer mechanism for the cryoprobe. However, when the radius of the cryoprobe is downscaled to 0.25 mm, the required heat transfer coefficient increases to 1800 W/(m^2·K). Furthermore, as mentioned above, the frozen region shrinks as the probe radius decreases. Therefore, to generate a frozen region of the same size, a much larger heat transfer coefficient is needed.

Fig. 11 shows the dimensional form of Fig. 8 using the thermophysical properties listed in Table 3. In relation to downscaling of the cryoprobe, Fig. 11 shows that the freezing limit lines shifted to the right, which indicates that a higher heat transfer coefficient is required to design a downscaled cryoprobe with the same cooling power as a larger cryoprobe.

7. Conclusions

In this study, a bioheat transfer analysis was performed to evaluate the performance of a miniaturized cryoprobe for cryosurgery. A one-dimensional axisymmetric freezing model was solved under convective heat transfer boundary condition, and dimensionless and dimensional solutions were derived. The major conclusions of this study are summarized as follows:

- The one-dimensional axisymmetric solutions were evaluated by comparing them with numerical simulation results obtained from other studies. The differences between the analytical solutions and the numerical results were found to be satisfactory from the viewpoint of discussing the general characteristics of this phenomenon. In addition, in the dimensionless case, the differences in the sizes of the frozen region were equal to or twice the characteristic length of bioheat transfer.
- By introducing steady-state surface temperature on the cryoprobe's surface, the fluid temperature and heat transfer coefficient were eliminated from the solutions. This transformation indicates that the steady-state surface temperature directly affects the size of the frozen region. Moreover, combination of the fluid temperature and the heat transfer coefficient occurs, which has same cooling effect.

Table 3
Thermophysical properties of soft biological tissue (Deng and Liu, 2005).

	Thermal conductivity k, W/(m·K)	Specific heat c, J/(kg·K)	Density ρ, kg/m^3	Blood perfusion rate ω_b, 1/s	Metabolic heat generation rate q_{met}, W/m^3
Frozen	2	1800	1000	–	–
Unfrozen	0.5	3600	1000	5×10^{-4}	4200

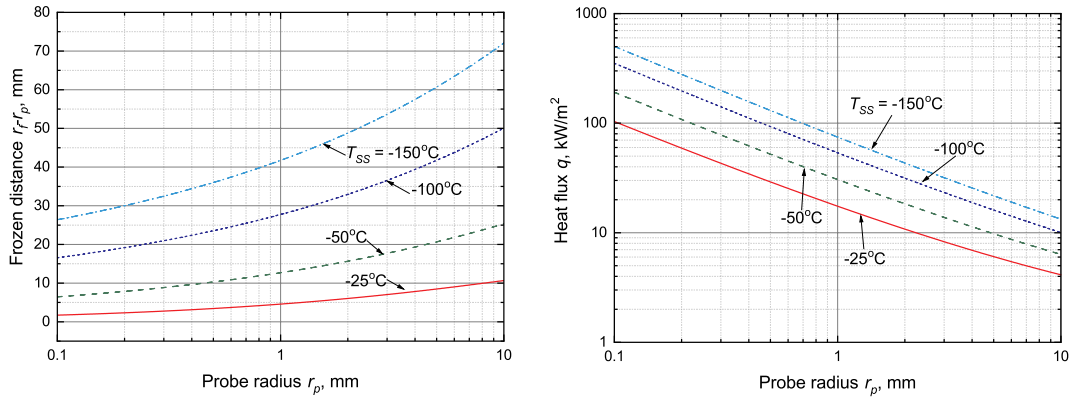

(a) Frozen distance (b) Heat flux

Fig. 9. Relationship between probe radius and (a) frozen distance and (b) heat flux.

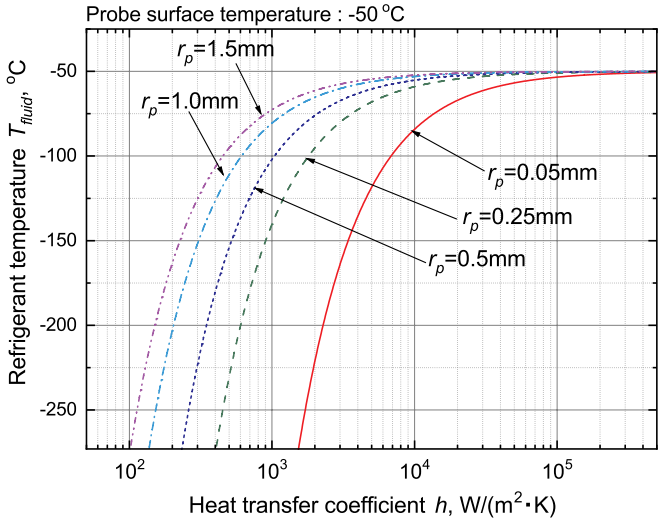

Fig. 10. Relationship between refrigerant temperature and heat transfer coefficient for probe surface temperature of −50 °C.

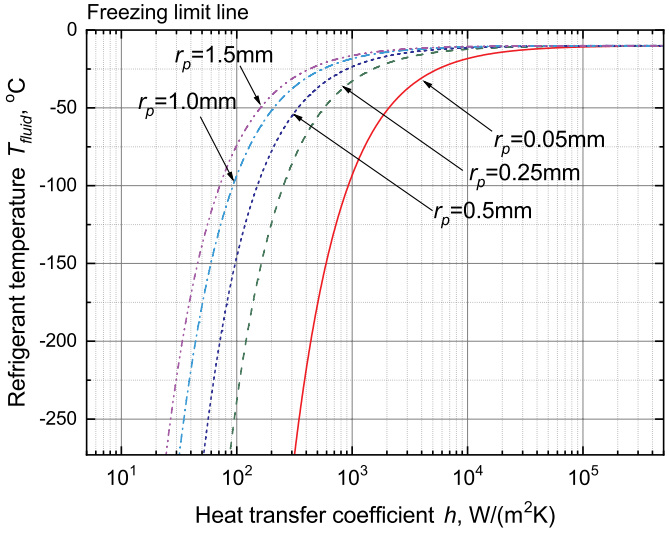

Fig. 11. Freezing limit for various probe radii in dimensional form.

- The relationship between the dimensionless frozen distance, heat flux, and probe radius was evaluated, and it was found that smaller cryoprobes require lower surface temperatures to generate the same frozen region size. Moreover, the dimensionless heat flux drastically increased as the dimensionless probe radius decreased. A smaller cryoprobe is required for a much larger heat transfer coefficient to produce low temperatures.
- The dimensional values were calculated using the derived equations. To generate probe surface temperature of −50 °C with fluid temperature of −100 °C, heat transfer coefficients of 450 W/(m^2·K) and 1800 W/(m^2·K) are required for cryoprobe radii of 1.5 mm and 0.25 mm, respectively.
- The concept of freezing limit was established using the derived solutions. The freezing limit describes the minimum requirement to freeze the tissue, which can be used to formulate guidelines for designing a cryoprobe.

The findings of this study were based on the assumption of one-dimensional axisymmetric geometry and steady-state condition, as well as simple relationships between the size of the frozen region, probe radius, refrigerant temperature, and heat transfer coefficient inside the cryoprobe. These relationships can be used as guideline for designing a cryoprobe.

Funding

This research did not receive any specific grant from funding agencies in the public, commercial or not-for-profit sectors.

References

Béita, M., Condé, H., 1972. Effects of local cooling upon conduction and synaptic transmission. Brain Res. 36 (1), 133–151.
Bischof, J., Christov, K., Rubinsky, B., 1993. A morphological-study of cooling rate response in normal and neoplastic human liver-tissue-cryosurgical implications. Cryobiology 30 (5), 482–492.
Chua, K.J., Chou, S.K., Ho, J.C., 2007. An analytical study on the thermal effects of cryosurgery on selective cell destruction. J. Biomech. 40 (1), 100–116.
Coleman, R.B., Richardson, R.N., 2005. A novel closed cycle cryosurgical system. Int. J. Refrig. 28 (3), 412–418.
Cooper, T.E., Trezek, G.J., 1971. Rate of lesion growth around spherical and cylindrical cryoprobes. Cryobiology 7 (4–6), 183–190.
Deng, Z.-S., Liu, J., 2005. Numerical simulation of selective freezing of target biological tissues following injection of solutions with specific thermal properties. Cryobiology 50 (2), 183–192.
Forest, V., Peoc'h, M., Campos, L., Guyotat, D., Vergnon, J.-M., 2006. Benefit of a combined treatment of cryotherapy and chemotherapy on tumour growth and late cryo-induced angiogenesis in a non-small-cell lung cancer model. Lung Canc. 54 (1), 79–86.
Fredrickson, K., Nellis, G., Klein, S., 2006. A design method for mixed gas Joule-Thomson refrigeration cryosurgical probes. Int. J. Refrig. 29 (5), 700–715.
Hafid, M., Lacroix, M., 2017. Fast inverse prediction of the freezing front in cryosurgery. J. Therm. Biol. 69, 13–22.
Hewitt, P.M., Zhao, J., Akhter, J., Morris, D.L., 1997. A comparative laboratory study of liquid nitrogen and argon gas cryosurgery systems. Cryobiology 35 (4), 303–308.

Hossain, S.M.C., Zhang, X., Haider, Z., Hu, P., Zhao, G., 2018. Optimization of prostatic cryosurgery with multi-cryoprobe based on refrigerant flow. J. Therm. Biol. 76, 58–67.
Jiji, L.M., Ganatos, P., 2009. Approximate analytical solution for one-dimensional tissue freezing around cylindrical cryoprobes. Int. J. Therm. Sci. 48 (3), 547–553.
Nabaei, M., Karimi, M., 2018. Numerical investigation of the effect of vessel size and distance on the cryosurgery of an adjacent tumor. J. Therm. Biol. 77, 45–54.
Nikolai, N.K., 2007. A history of cryosurgery: its development and future. J. Am. Coll. Surg. 204 (2), 314–324.
Okajima, J., Maruyama, S., Takeda, H., Komiya, A., 2009. Dimensionless solutions and general characteristics of bioheat transfer during thermal therapy. J. Therm. Biol. 34 (8), 377–384.
Okajima, J., Komiya, A., Maruyama, S., 2014a. 24-gauge ultrafine cryoprobe with diameter of 550μm and its cooling performance. Cryobiology 69 (3), 411–418.
Okajima, J., Komiya, A., Maruyama, S., 2014b. Evaluation of characteristics of phase change heat transfer in ultrafine cryoprobe. J. Flow Control Meas. Vis. 2 (2), 55–66.
Okajima, J., Komiya, A., Maruyama, S., 2014c. Experimental and numerical evaluation of small-scale cryosurgery using ultrafine cryoprobe. J. Nanotechnol. Eng. Med. 4 (4), 041009.
Okajima, J., Jeong, S., Maruyama, S., 2018. Evaluation of cooling performance of ultrafine cryoprobes: effect of probe structure on thermodynamic properties of refrigerant. Int. J. Air Cond. Refrig. 26 (2), 1850020.
Pennes, H.H., 1948. Analysis of tissue and arterial blood temperatures in the resting human forearm. J. Appl. Physiol. 1 (2), 93–122.
Popken, F., Seifert, J.K., Engelmann, R., Dutkowski, P., Nassir, F., Junginger, T., 2000. Comparison of iceball diameter and temperature distribution achieved with 3-mm accuprobe cryoprobes in porcine and human liver tissue and human colorectal liver metastases in vitro. Cryobiology 40 (4), 302–310.
Rabin, Y., Shitzer, A., 1998. Numerical solution of the multidimensional freezing problem during cryosurgery. J. Biomech. Eng. 120 (1), 32–37.
Shimizu, T., 2004. MRI-imaging guided percutanous intersitial cryoabration. J. Heat Transf. Soc. Jpn. 43 (180), 11–15 (in Japanese).
Takeda, H., Maruyama, S., Okajima, J., Aiba, S., Komiya, A., 2009. Development and estimation of a novel cryoprobe utilizing the Peltier effect for precise and safe cryosurgery. Cryobiology 59 (3), 275–284.
Zhang, J.-x., Ni, H., Harper, R.M., 1986. A miniaturized cryoprobe for functional neuronal blockade in freely moving animals. J. Neurosci. Methods 16 (1), 79–87.
Zhang, J., Sandison, G.A., Murthy, J.Y., Xu, L.X., 2005. Numerical simulation for heat transfer in prostate cancer cryosurgery. J. Biomech. Eng. 127 (2), 279–294.
Zhao, G., Zhang, H.-F., Guo, X.-J., Luo, D.-W., Gao, D.-Y., 2007. Effect of blood flow and metabolism on multidimensional heat transfer during cryosurgery. Med. Eng. Phys. 29 (2), 205–215.